Article

Extended Critical Damping Adjustment Method for Electromagnetic Transients Simulation in Power Systems

Qiang Li [1], Yong Wang [1,2,*] , Huaxing Rao [1], Lei Zhang [1], Jing Ye [1], Xiaolin Lei [1] and Bingwen Chen [1]

[1] College of Electrical Engineering & New Energy, China Three Gorges University, Yichang 443002, China; 2016120506258@ctgu.edu.cn (Q.L.); 2016120506186@ctgu.edu.cn (H.R.); leizhang3188@163.com (L.Z.); yejing2000310@163.com (J.Y.); 2016120506216@ctgu.edu.cn (X.L.); 201708520721002@ctgu.edu.cn (B.C.)

[2] China Shanghai Administration Bureau of State Grid Operation Company, Shanghai 200000, China

* Correspondence: yongwang2015wy@163.com; Tel.: +86-021-5172-0605

check for updates

Abstract: Numerical oscillation is a common phenomenon in the current electromagnetic transient digital simulation in power systems. From the origin of the numerical oscillation, we proposed an extended critical damping adjustment method (ECDA) to solve the numerical oscillation problem in this paper, after inspired by the critical damping adjustment method (CDA). ECDA was composed of a class of new low-order, L-stable linear multistep and implicit trapezoidal integration methods. ECDA used two-half-step, three-step or four-steps linear multistep method to perform numerical integrations when experienced with sudden changes, and the implicit trapezoidal integration method was still used under normal conditions. The numerical simulation results of the typical electromagnetic transient examples show that the ECDA could completely eliminate the numerical oscillation, and it had higher computational accuracy than the CDA.

Keywords: electromagnetic transients simulation; linear multistep formulae; extended critical damping adjustment; numerical oscillation

---

1. Introduction

The phenomenon of numerical oscillations is a common problem in the electromagnetic transient simulation in power systems [1], which is due to the reason that the numerical integration algorithm in power-system transient simulation calculation is mainly an implicit trapezoidal integration method [1,2]. However, the implicit trapezoidal integration method is not L-stable and does not have the ability to eliminate numerical oscillations [3]. Therefore, the traditional power-system electromagnetic transient simulation software, such as EMTP 3.0, use critical damping adjustment (CDA) to eliminate numerical oscillations [4,5].

The CDA method is essentially a combined integration algorithm. The core step of the CDA method is to use two-half-step backward Euler method for numerical integrations to eliminate numerical oscillations [6,7]. The backward Euler method is a one-step, low-order, L-stable numerical integration algorithm, which eliminates numerical oscillations from its source.

In addition, other schemes for solving the problem of numerical oscillations indirectly use different technical approaches to approximating non-state variables for obtaining their "real" values [1,5]. For example, PSCAD version 4.0 uses a half-step interpolation algorithm to eliminate numerical oscillations, but this method is only suitable for offline simulations [8].

Based on the state space method in electromagnetic transient simulations [9,10], we proposed an extended critical damping adjustment method (ECDA), in this paper, to solve the problem of

numerical oscillations directly from the origin of the numerical oscillations. The core idea of the ECDA is similar to that of CDA. The difference between these two methods lies in the use of a new class of low-order linear multistep formulae (L_2MF) to avoid the numerical oscillations. The absolute value of the main coefficient of the local truncation error of a new four-step L_2MF using Chebyshev grid points was smaller than that of the backward Euler method. The pure L_2MF method and the implicit trapezoidal integration method were used to form the ECDA to solve numerical examples. The simulation results show that the L_2MF method can effectively avoid the numerical oscillations, and also indirectly show that the ECDA has a better simulation effect than the CDA in theory, and hence has the potential applications in EMTP-type programs.

2. A New Class of Linear Multistep Formulae

2.1. Construction of a New Class of Linear Multistep Formulae by Classic Differential Quadrature

The initial-value problem of an ordinary differential equation was shown in the following:

$$\begin{cases} \dot{x}(t) = f(t, x) \\ x(t = 0) = x_0 \end{cases} \tag{1}$$

where t is time and x is a one-dimensional variable; $f(t, x)$ is a function of the time t and the variable x; and x_0 is the initial value of an unknown state variable.

One of main methods for solving the initial-value problem, as indicated in Equation (1), is the use of classical linear multistep formulae (LMF) [11], and one kind of the LMF is the following backward differentiation formula (BDF), which was described as following:

$$\sum_{i=0}^{s} \alpha_i x_{n+i} = h f_{n+s} \tag{2}$$

where s is the number of steps; α_i is integration coefficient; h denotes the integration step; $x_{n+i} \approx x(t_{n+i})$ is the approximate value of a state variable at a time point t_{n+i}; and $f_{n+s} = f(t_{n+s}, x_{n+s})$.

Obviously, when s takes one, Equation (2) is the first-order backward Euler method that is A-stable and L-stable. Based on the traditional BDF, new linear multistep methods were constructed as follows:

$$\sum_{i=0}^{s} \widetilde{\alpha}_i x_{n+i} = h \beta_s f_{n+s} \tag{3}$$

where $\widetilde{\alpha}_i$ and β_s are integration coefficients of new LMF, respectively.

In order to obtain the unknown integration coefficients of new LMF, we similarly used s-stage s-order time-domain differential quadrature method (DQM) [12–14] to solve Equation (1). For any time-step ($h = t_{n+1} - t_n$), we have the following equation:

$$G \begin{bmatrix} \widetilde{x}_{n+1} \\ \vdots \\ \widetilde{x}_{n+s} \end{bmatrix} + G_0 x_n = h \begin{bmatrix} f(\widetilde{t}_1, \widetilde{x}_{n+1}) \\ \vdots \\ f(\widetilde{t}_s, \widetilde{x}_{n+s}) \end{bmatrix} \tag{4}$$

where $c_i = (\widetilde{t}_i - t_n)/h, i \in (0, s)$ is the non-equidistant grid point, which is distributed over the regularization interval $[0, 1]$; $\widetilde{t}_0 = t_n$ is a time-starting point; $\widetilde{t}_s = t_{n+1}$ is a time-end point; $\widetilde{t}_i = t_n + c_i h, i \in (1, s)$ are internal points; and $\widetilde{x}_{n+i} \approx x(\widetilde{t}_i)$ is the approximate value of a state variable at a time-internal point $\widetilde{t}_i$.

$$G = \begin{bmatrix} g_{11} & \cdots & g_{1s} \\ \vdots & \ddots & \vdots \\ g_{s1} & \cdots & g_{ss} \end{bmatrix}, G_0 = \begin{bmatrix} g_{10} \\ \vdots \\ g_{s0} \end{bmatrix} \tag{5}$$

where G is called the weighted coefficient matrix of DQM, and the calculation formulae of each element in G is given in Reference [15] $G_0 = -Ge$, where e is the column vector with each element equaling to one.

In Equation (4), the grid point distribution has to be a non-equidistant grid, including Chebyshev grid, Chebyshev-Gauss-Lobatto grid, and Legendre grid [16]. In this paper, we used the DQM with Chebyshev grid points [16] for constructing the new LMF. Suppose:

$$\widetilde{\alpha}_i = g_{si}/g_{ss}, i \in (0, s), \beta_s = \sum_{i=1}^{s} i\widetilde{\alpha}_i \tag{6}$$

where $\widetilde{\alpha}_s = 1$.

As an example, the new three-step LMF using Chebyshev grid points was shown below:

$$\frac{15 - 4\sqrt{2}}{9}hf_{n+3} = -\frac{1}{9}x_n + \frac{4\sqrt{2} - 4}{9}x_{n+1} - \frac{4\sqrt{2} + 4}{9}x_{n+2} + x_{n+3} \tag{7}$$

The new four-step LMF using Chebyshev grid points is as follows:

$$\frac{108 - 32\sqrt{3}}{57}hf_{n+4} = \frac{1}{19}x_n + \frac{16\sqrt{3} - 32}{57}x_{n+1} + \frac{4}{57}x_{n+2} - \frac{16\sqrt{3} + 32}{57}x_{n+3} + x_{n+4} \tag{8}$$

In addition, the backward Euler method is obtained when s takes one in Equation (3) regardless of the kind of the used grid. Similarly, when s takes two, we get the second-order Gear method.

2.2. The Compatibility and Convergence of the L_2MF

The new linear multistep methods have practical applications only if they satisfy compatibility and convergence. Therefore, according to Equation (3), the first-characteristic polynomial and the second-characteristic polynomial of z were as follows [17]:

$$\rho(z) = \sum_{i=0}^{s} \widetilde{\alpha}_i z^i, \sigma(z) = \beta_s z^s \tag{9}$$

where $\rho(1) = 0$ and $\rho'(1) = \sigma(1)$. Therefore, the new linear multistep methods satisfy the compatibility. Suppose $\rho(z) = 0$. A unique root modulus is $|z_1| = 1$, and the rest of the roots' modulus satisfies $|z_i| < 1, i \in (2, s)$. Therefore, it also meets the root condition. Since the new linear multistep formulae satisfy both the compatibility and the root condition, the new linear multistep formulae are convergent according to the Dahlquist equivalence theorem [17,18].

2.3. Stability of the L_2MF

For the stability analysis of the new linear multistep method, the following standard test equations can be considered:

$$\begin{cases} \frac{dx}{dt} = \lambda x \\ x(0) = 1 \end{cases} \tag{10}$$

where $\mathrm{Re}(\lambda) < 0$.

According to Equation (3), the corresponding characteristic equation was obtained:

$$\rho(z) - q\sigma(z) = 0, q = \lambda h \tag{11}$$

where the stability domains of different s values in Equation (3), supposing, were shown in Figures 1 and 2. In Figures 1 and 2, the outside regions of boundary curves were the stability domain of the new LMF. Obviously, the numerical stability regions of the new linear multistep methods contained the entire left-half complex plane, so the new LMF were A-stable.

According to the Dahlquist barriers theorem [19], new two-step LMF were second-order methods, and other LMF were first-order methods. The main coefficient of the local truncation error for the three-step LMF and the four-step LMFs are -0.6683 and -0.3009, respectively.
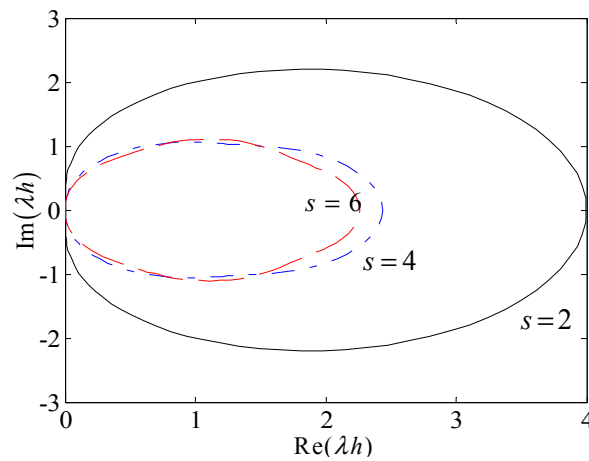

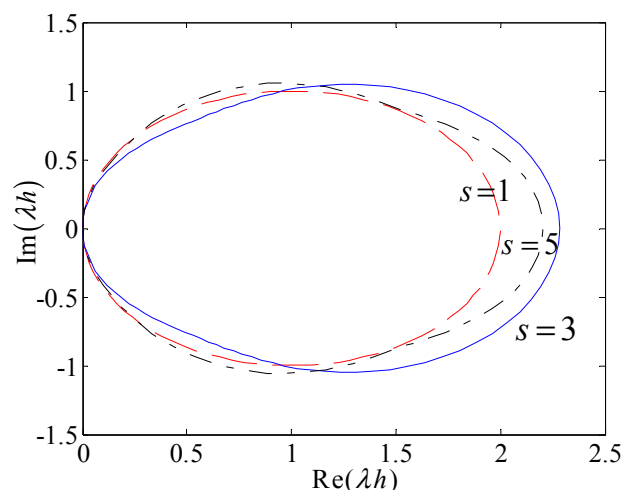**Figure 1.** Stability region of new linear multistep formulae (LMF) for even numbers of *s*.

Figure 2. Stability region of new LMF for odd numbers of *s*.

In addition, Equation (9) was substituted into Equation (3); hence the following equation was obtained:

$$\frac{x_{n+s}}{x_{n+s-1}} = \frac{-\widetilde{\alpha}_{s-1}}{1 - \beta_s \lambda h} + \frac{-\sum_{i=0}^{s-2} \widetilde{\alpha}_i \frac{x_{n+i}}{x_{n+s-1}}}{1 - \beta_s \lambda h} \tag{12}$$

where $|x_{n+s}/x_{n+s-1}| \rightarrow 0$ if $\text{Re}(\lambda h) \rightarrow -\infty$. Therefore, the new linear multistep formulae were L-stable [19].

In summary, the new linear multistep methods are low-order methods. So it is named as low-order LMF (L_2MF) method. In numerical stability, the L_2MF method was both A-stable and L-stable. Therefore, compared with the A-stable second-order implicit trapezoidal integration method, the L_2MF method has strong damping characteristics, which can effectively suppress the numerical oscillations, and hence is suitable for electromagnetic transient simulations in power systems.

3. Extended Critical Damping Adjustment Scheme

From the above analysis, it can be seen that the L_2MF method belongs to the numerical methods with low-order and strong numerical stability. For this purpose, it is necessary to combine the implicit trapezoidal integration method, which is widely used in electromagnetic transient calculation, to calculate the implicit trapezoidal integration method under normal circumstances, and to switch to L_2MF only when the system is mutated, such as switch operation and line fault. In practice, we can use the same method of auxiliary detection mutation as the CDA method and the algorithm switching strategy. Because the absolute value of the local truncation error of the four-step L_2MF method is smaller than that of the backward Euler method (the absolute value of the main coefficient of local truncation error is 0.5), it was recommend that a four-step L_2MF method and an implicit trapezoid integration method are used to form that combined integration algorithm for the electromagnetic transient simulation in power systems.

In the new combination integration scheme, the implicit trapezoidal integration method had the ability of self-starting computation, and the L_2MF method did not have the self-starting calculation ability, which needed a startup algorithm for independent calculation. The starting numerical method used in this paper was explicit Euler method (forward Euler method). Figure 3 is a flow chart of electromagnetic transient simulation in power systems on a basis of extended CDA method (ECDA).
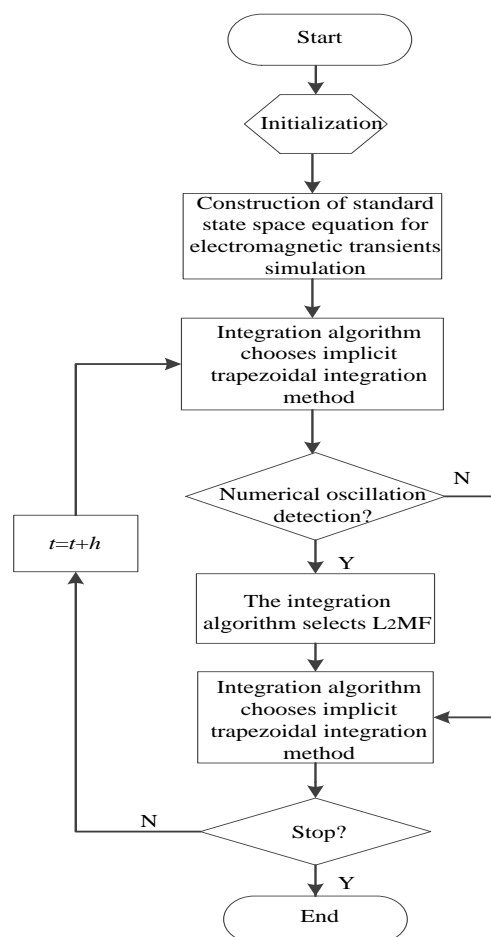
Figure 3. Flow chart of electromagnetic transient simulation in power systems on a basis of extended critical damping adjustment method (ECDA).

The combined integration algorithm proposed in this paper was a class of algorithms, and the combination algorithm was the CDA method when *s* takes one. Therefore, the new combination algorithm proposed in this paper was also named as the extended CDA method.

4. Simulation Examples
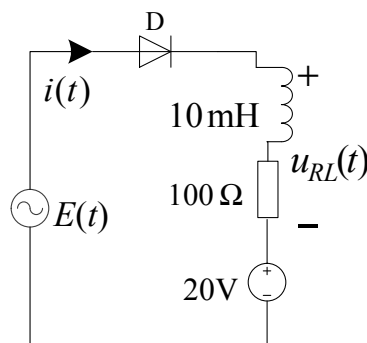
4.1. Simulation of Half-Wave Rectifier Circuit

The example is half-wave rectifier circuit. As shown in Figure 4, the excitation source was an ideal sinusoidal voltage source $E(t) = 100\sqrt{2}\sin(100\pi t)$. The value of the DC voltage source is 20 V . The first-order differential equation for the circuit is as follows:

$$\frac{\mathrm{d}i}{\mathrm{d}t} = \frac{1}{L}(E(t) - d(t) - 20 - Ri) \tag{13}$$

where *i* is the current, *R* is the resistance, and *L* is the inductance.

A three-step L_2MF method and an implicit trapezoidal integration method were used to solve Equation (13), and the integration step in this case was set to $h = 0.1$ ms. The simulation results are shown in Figure 5.

Figure 4. Half-wave rectifier circuit. D represents the diode, which is an ideal switching device with voltage described as $d(t)$. $u_{RL}(t)$ denotes a load voltage.
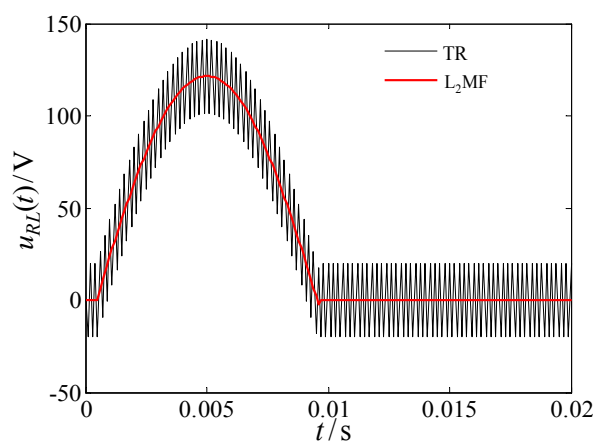
Figure 5. Load voltage calculated by the three-step low-order linear multistep formulae (L_2MF) method and the implicit trapezoidal integration method(TR).

As shown in Figure 5, since the three-step L_2MF method was L-stable and had a strong damping characteristic, which could suppress the numerical oscillations of non-state variables when the diode D turned on. In contrast, the implicit trapezoidal integration method used in the style of EMTP produces

a serious numerical oscillation when the network changed suddenly. It is worth mentioning that the implicit trapezoidal integration method directly used for solving Equation (13) did not produce numerical oscillations.

4.2. Simulation of High-Voltage Transmission Line without Load Being Switched-In Suddenly

This example is an electromagnetic transient simulation of a single-phase middle-long transmission line with distributed parameters. The initial phase of the sinusoidal voltage source was $\varphi_0 = 90°$. The other parameters of the transmission line were given in Figure 6.
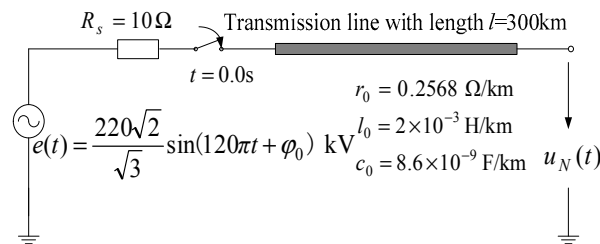
Figure 6. Schematic diagram of a single-phase high-voltage overhead transmission line without load being switched-in suddenly.

The mathematical model of the electromagnetic transient process for the transmission line was described by the telegraph equation as follows:

$$\begin{cases} -\dfrac{\partial v(y,t)}{\partial y} = l_0 \dfrac{\partial i(y,t)}{\partial t} + r_0\ i(y,t) \\ -\dfrac{\partial i(y,t)}{\partial y} = c_0 \dfrac{\partial v(y,t)}{\partial t} + g_0 v(y,t) \end{cases} \tag{14}$$

where y and t are the spatial variables of the length and the time variable, respectively; $v(y,t)$ and $i(y,t)$ denote the changes of the voltage and the current with respect to the space and the time, respectively; l_0, c_0, r_0 and g_0 are the unit parameters of inductance, capacitance, resistance, and susceptance, respectively.

In this paper, we adopt the time-domain method to settle the telegraph Equation (14). First, in order to obtain the voltage and current variables along the transmission line, we decompose the whole line into N sub-intervals uniformly, as is shown in Figure 7. Supposing the total length of the transmission line is l, we define: the length of each small interval is $\Delta y = l/N$. Let v_k denote the voltage at the point, where $y = y_k = k \cdot \Delta y, k \in (0, N)$; $i_k, k \in (1, N)$ is the current from the point y_{k-1} to the point y_k; and i_0 and i_{N+1} are the currents of two terminals in the line, respectively.

Furthermore, we apply the fourth-order accuracy interpolation formula to do spatial discretization of the telegraph equation [20]:

$$\theta_1 \left.\frac{\partial \lambda_j(y)}{\partial y}\right|_{j=k-1} + \theta_2 \left.\frac{\partial \lambda_j(y)}{\partial y}\right|_{j=k} + \theta_1 \left.\frac{\partial \lambda_j(y)}{\partial y}\right|_{j=k+1} = \frac{\lambda_k - \lambda_{k+1}}{\Delta y} \tag{15}$$

where λ denotes v or i; θ_1 and θ_2 are the constant coefficients decided by the interpolation formula; and $\theta_1 = 1/24, \theta_2 = 1 - 2\theta_2$.

Substituting Equation (15) into the telegraph equation (Equation (14)), we obtained the spatial discretization form of the telegraph equation as follows:

$$\begin{cases} \frac{v_k - v_{k+1}}{\Delta y} = \theta_1 \left(l_0 \dot{i}_{k-1} + r_0 i_{k-1} \right) + \theta_2 \left(l_0 \dot{i}_k + r_0 i_k \right) + \theta_1 \left(l_0 \dot{i}_{k+1} + r_0 i_{k+1} \right), k \in (1, N-2) \\ \frac{i_k - i_{k+1}}{\Delta y} = \theta_1 \left(c_0 \dot{v}_{k-1} + g_0 v_{k-1} \right) + \theta_2 \left(c_0 \dot{v}_k + g_0 v_k \right) + \theta_1 \left(c_0 \dot{v}_{k+1} + g_0 v_{k+1} \right), k \in (1, N-1) \end{cases} \tag{16}$$

For the head-end and the tail-end of the line, we used the second-order accuracy interpolation formula [20] to do spatial discretization as follows:

$$\begin{cases} \frac{v_0 - v_1}{\Delta y} = \theta_3 \left(l_0 \dot{i}_1 + r_0 i_1 \right) + \theta_1 \left(l_0 \dot{i}_2 + r_0 i_2 \right) \\ \frac{i_0 - i_1}{\Delta y} = \theta_4 \left(c_0 \dot{v}_0 + g_0 v_0 \right) + \theta_1 \left(c_0 \dot{v}_1 + g_0 v_1 \right) \end{cases}, \tag{17}$$

and

$$\begin{cases} \frac{v_{N-1} - v_N}{\Delta y} = \theta_3 \left(l_0 \dot{i}_N + r_0 i_N \right) + \theta_1 \left(l_0 \dot{i}_{N-1} + r_0 i_{N-1} \right) \\ \frac{i_N - i_{N+1}}{\Delta y} = \theta_4 \left(c_0 \dot{v}_N + g_0 v_N \right) + \theta_1 \left(c_0 \dot{v}_{N-1} + g_0 v_{N-1} \right) \end{cases} \tag{18}$$

where $\theta_3 = 1 - \theta_1$ and $\theta_4 = 1/2 - \theta_1$.

Considering the boundary conditions of both ends of the transmission line, we obtained the following equations by combining Equations (16)–(18):

$$K\dot{x} + \rho x + \omega(t) = 0 \tag{19}$$

where $K, \rho \in R^{(2N+1) \times (2N+1)}$ is the constant coefficient matrix; $\omega(t)$ is the input excitation source for the transmission line; and where:

$$x = \begin{bmatrix} v_0 & v_1 & \cdots & v_N & i_1 & \cdots & i_N \end{bmatrix}^{\mathrm{T}} \tag{20}$$

$$\omega(t) = [-i_0, 0, \cdots, 0, i_{N+1}, 0, \cdots, 0]^{\mathrm{T}} \tag{21}$$

$$K = \begin{bmatrix} a_4 & a_1 & & & & & & & 0 \\ a_1 & a_2 & \ddots & & & & & & \\ & \ddots & \ddots & \ddots & & & & & \\ & & \ddots & a_2 & a_1 & & & & \\ & & & a_1 & a_4 & & & & \\ & & & & & b_3 & b_1 & & \\ & & & & & b_1 & b_2 & \ddots & \\ & & & & & & \ddots & \ddots & b_1 \\ 0 & & & & & & & b_1 & b_3 \end{bmatrix} \tag{22}$$

$$\rho = \begin{bmatrix} \beta_4 & \beta_1 & & & & 1 & & & \\ \beta_1 & \beta_2 & \ddots & & & -1 & 1 & & \\ & \ddots & \ddots & \ddots & & & \ddots & \ddots & \\ & & \ddots & \beta_2 & \beta_1 & & & -1 & 1 \\ & & & \beta_1 & \beta_4 & & & & -1 \\ -1 & 1 & & & & \phi_3 & \phi_1 & & \\ & -1 & 1 & & & \phi_1 & \phi_2 & \ddots & \\ & & \ddots & \ddots & & & \ddots & \ddots & \phi_1 \\ & & & -1 & 1 & & & \phi_1 & \phi_3 \end{bmatrix} \tag{23}$$

where

$$a_j = c_0 \cdot \Delta y \cdot \theta_j, \ b_j = l_0 \cdot \Delta y \cdot \theta_j, \ \beta_j = g_0 \cdot \Delta y \cdot \theta_j, \ \phi_j = r_0 \cdot \Delta y \cdot \theta_j, \ (j = 1, 2, 3, 4) \tag{24}$$
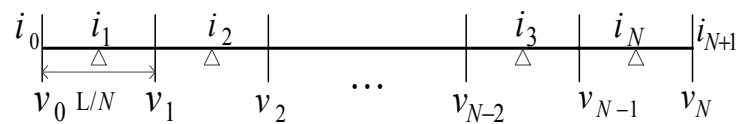
Figure 7. A piecewise model of a transmission line.

The four-step L_2MF method and the implicit trapezoidal integration method were used to solve Equation (19), and the integration step of the simulation test was $h = 1$ μs for both L_2MF and the implicit trapezoidal integration method. Moreover, the transmission line was uniformly divided into $N = 50$ sections. The simulation results are shown in Figure 8, and Figure 9 is an enlargement of Figure 8.
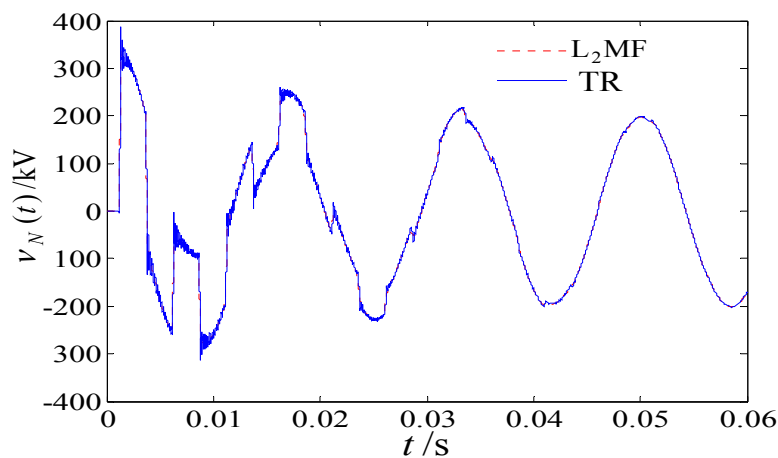

Figure 8. Terminal voltage of the transmission line calculated by the four-step L_2MF method and the implicit trapezoidal integration method.
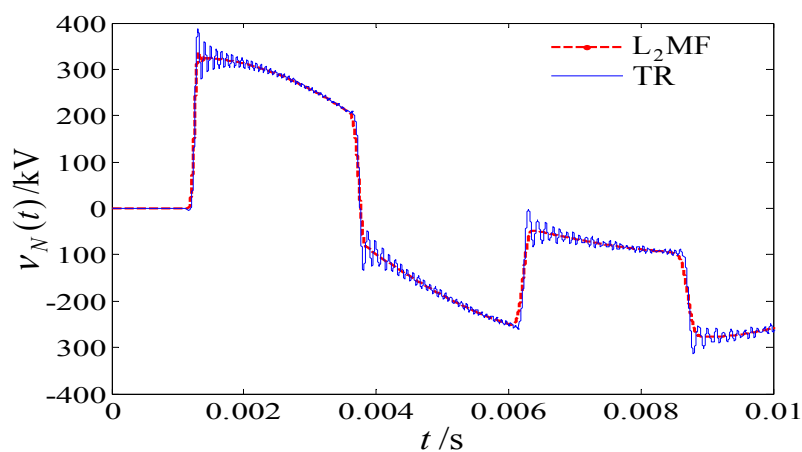
Figure 9. An enlargement of Figure 8.

As shown in Figures 8 and 9, the calculation results of the four-step L_2MF method were basically consistent with the second-order the implicit trapezoidal integration method. In the moment of the circuit closing, the implicit trapezoidal integration method had a continuous numerical oscillation due to the lack of L-stability. On the contrary, the four-step L_2MF method was L-stable, and therefore had strong damping property, which effectively inhibited the numerical oscillations.

4.3. Very Fast Transient Overvoltage Calculation

In this case, we simulate a situation when the disconnector of 550 kV gas insulated switchgear (GIS) acts on the no-load bus. During this process, very fast transient overvoltage (VFTO) is caused by slow contact action and poor arc-extinguishing performance of switch [21,22]. Figure 10 is a simplified equivalent circuit diagram for this process. In Figure 10, $e(t)$ is the AC power supply; L_t and C_t are used to simulate the lumped inductance and capacitance parameters of the transformer and other equipment. DS is the isolation switch, and its mathematical model can be established by a nonlinear time-varying resistance. C_r is the lumped ground capacitance with initial voltage to simulate the residual charge; L_1 and L_2 are import and export short bus, respectively. All parameters of this example in Figure 10 were taken from Reference [23].
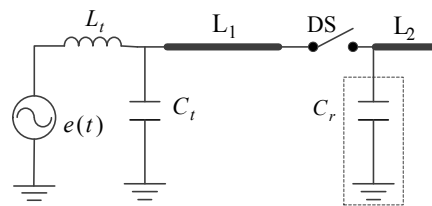
Figure 10. A simplified GIS (gas insulated switchgear) for very fast transient overvoltage (VFTO) simulation.

The mathematical model of the VFTO simulation was established by using the telegraph equation for the short bus L_1 and L_2. The short bus, L_1, was uniformly divided into $N_1 = 20$ sections, and $N_2 = 7$ of the short bus L_2 was selected. The following ordinary differential equations were obtained by the interpolation formulae [20]:

$$\dot{x} = Ax + \delta(t) \tag{25}$$

As the simulation time-step of VFTO was nanosecond scaled, it could be considered that A was the constant matrix in a time-step and $\delta(t)$ was the incentive source of VFTO.

The four-step L_2MF and the implicit trapezoidal integration method were used to solve Equation (16). The integration step of the implicit trapezoidal integration method was $h = 1$ ns and a smaller integration step of L_2MF was $h = 0.1$ ns. The simulation results in this case are shown in Figure 11.

In this simulation test, the simulation time-step of VFTO was nanosecond scaled, which accurately simulated the change rule of the open-circuit voltage $u(t)$ at the end of the line. Neither of these methods produced numerical oscillations, and the waveforms of VFTO for both the methods were almost the same.
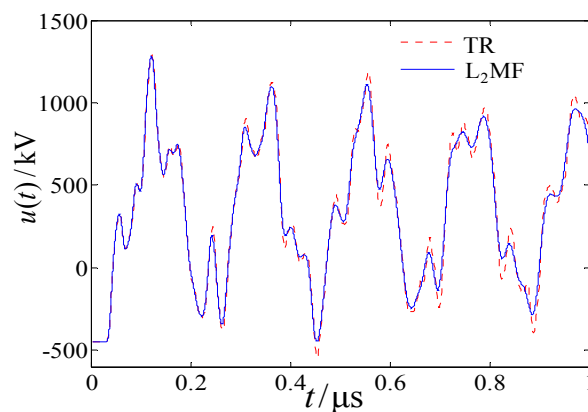

Figure 11. VFTO calculated by the four-step L_2MF method and the TR method.

4.4. RC Series Circuit Simulation Calculation

This example is the series of a *RC* circuit, as shown in Figure 12. Figure 12a is a basic linear *RC* series test circuit. Figure 12b is the excitation voltage source waveform. The exact solution of the capacitor voltage in the circuit was given as follows:

$$u_{\text{C}}(t) = \frac{1}{\Delta t}\left\{[t - \tau(1 - \text{e}^{-t/\tau})] - [t - \Delta t - \tau(1 - \text{e}^{-(t-\Delta t)/\tau})]u(t - \Delta t)\right\} \tag{26}$$

where $\Delta t = 0.1$ ms; a time constant, $\tau = RC$, τ is 0.1 ms; and $u(t - \Delta t)$ is a delayed unit-step signal.
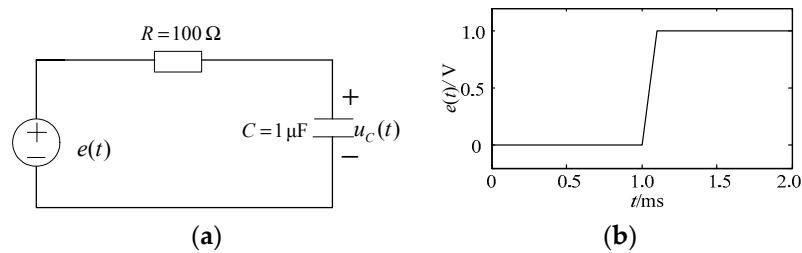
Figure 12. *RC* (resistance and capacitor) series test circuit and its excitation source. (**a**) *RC* series test circuit; and (**b**) excitation source waveform in the *RC* test circuit.

In this paper, the four-step L$_2$MF and the backward Euler method were used to solve the voltages at both the ends of the capacitor. The calculated time-step of the two algorithms was both $h = 0.1$ ms. The absolute error curve of the calculation results solved with the use of the two algorithms is shown in Figure 13. As shown in Figure 13, the calculation error of the four-step L$_2$MF was smaller than that of the backward Euler method. This is because, although both of them were first-order, the absolute value of the local phase error of the four-step L$_2$MF method was smaller than that of the backward Euler method. This example also indirectly verifies that the calculation effect of the ECDA combined with the four-step L$_2$MF and the implicit trapezoidal integration method was better than that of the CDA.
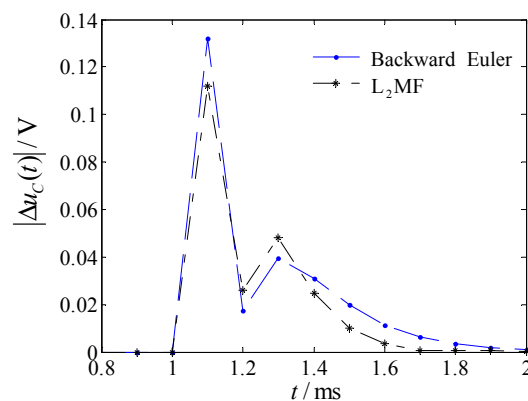
Figure 13. Computation errors of the L$_2$MF and backward Euler algorithms as a function of time.

5. Conclusions

Based on the traditional LMF, a class of low-order LMF was derived by the classic differential quadrature method. The L$_2$MF method had L-stability, and the absolute value of the basic coefficient of the truncation error of four-step L$_2$MF was smaller than that of the backward Euler method. Inspired by the CDA method, we proposed ECDA for electromagnetic transient simulation, which used the implicit trapezoidal integration method to perform integration operation under normal circumstances and

switched the integration algorithm to the four-step L_2MF method only when the network changed. The simulation results of the simple L_2MF method and the implicit trapezoidal integration method showed that the L_2MF method could avoid the numerical oscillation completely, and the ECDA had a better simulation effect than the CDA. The next step will apply the ECDA in EMTP-type programs.

Author Contributions: Y.W. proposed the methods and derived the equations; Y.W. and Q.L. performed the numerical simulations; L.Z., J.Y., X.L. and H.R. analyzed the simulation results and given the conclusions; L.Z., J.Y. and B.C. discussed the numerical results and provided useful suggestions on the overall organization of the paper; Y.W. and Q.L. wrote the paper.

References

1. Ji, Y.; Xu, J.; Xu, Y.; Zhao, C. Design of damping circuit for depressing numerical oscillation in interpolation-free simulation environment. *Electr. Power Autom. Equip.* **2016**, *36*, 143–149.
2. Chi, Y.; Shu, D.; Zhang, C.; Wei, L.; Jiang, Q. A parameterized rational-fraction fitting algorithm for numerical oscillation suppression in weak AC grid. *Power Syst. Technol.* **2016**, *40*, 1792–1796.
3. Yang, M.; Wang, F. 2-stage 3-order diagonally implicit Runge-Kutta method for electromagnetic transient calculation. *Power Syst. Protect. Control* **2017**, *45*, 68–73.
4. Noda, T.; Takenaka, K.; Inoue, T. Numerical integration by the 2-stage diagonally implicit Runge-Kutta method for electromagnetic transient simulations. *IEEE Trans. Power Deliv.* **2009**, *24*, 390–399. [CrossRef]
5. Shang, Y.; Yu, Y.M.; Zou, Z.Y.; Li, F.J.; Chen, B. An advanced method of non-linear circuit eliminating numerical oscillation in electromagnetic transient simulation. *Power Syst. Protect. Control* **2011**, *39*, 142–146.
6. Lin, J.; Marti, J.R. Implementation of the CDA procedure in the EMTP. *IEEE Trans. Power Syst.* **1990**, *5*, 394–402.
7. Marti, J.R.; Lin, J. Suppression of numerical oscillation in the EMTP. *IEEE Trans. Power Syst.* **1989**, *4*, 739–747. [CrossRef]
8. Watson, N.; Arrillaga, J. *Power Systems Electromagnetic Transients Simulation*; IET Press: London, UK, 2003; pp. 221–230.
9. Wang, C.; Li, P.; Wang, L. Progresses on algorithm of electromagnetic transient simulation for electric power system. *Autom. Electr. Power Syst.* **2009**, *33*, 97–103.
10. Ji, F.; Wei, X.; Wu, X.; Liu, J.; Xu, W. State space method to analyze the electromagnetic transient of linear switching circuit. *Proc. CSEE* **2016**, *36*, 6028–6037.
11. Gear, C.W. *Numerical Initial Value Problems in Ordinary Differential Equations*; Prentice Hall: Upper Saddle River, NJ, USA, 1971.
12. Bellman, R.; Casti, J. Differential quadrature and long-term integration. *J. Math. Anal. Appl.* **1971**, *34*, 235–238. [CrossRef]
13. Wang, F.; Liao, X.; Xie, X. Stability Analysis and Order Improvement for Time Domain Differential Quadrature Method. *Adv. Appl. Math. Mech.* **2016**, *8*, 128–144.
14. Wang, F.; Wang, Y. A Coupled Pseudospectral-Differential Quadrature Method for a Class of Hyperbolic Telegraph Equations. *Math. Probl. Eng.* **2017**, *2017*, 9013826. [CrossRef]
15. Quan, J.R.; Chang, C.T. New insights in solving distributed system equations by the quadrature methods, Part I: Analysis. *Comput. Chem. Eng.* **1989**, *13*, 779–788. [CrossRef]
16. Wang, F.; Liao, X.; Xie, X. Characteristics of the Differential Quadrature Method and Its Improvement. *Math. Probl. Eng.* **2015**, *2015*, 657494. [CrossRef]
17. Brugnano, L.; Trigiante, D. Boundary value methods: The third way between linear multistep and Runge-Kutta methods. *Comput. Math. Appl.* **1998**, *36*, 269–284. [CrossRef]
18. Liu, D.; Yang, D. A linear 3-step formula of 3-order with a large absolutely stable region. *J. Panzhihua Univ.* **2008**, *6*, 66–69.
19. Yuan, Z.; Fei, J.; Liu, D. *Numerical Solution of the Initial Value Problem of Stiff Ordinary Differential Equations*; Science Press: Beijing, China, 1987.

20. Cangellaris, A.C.; Pasha, S.; Prince, J.L.; Celik, M. A new discrete transmission line model for passive model order reduction and macromodeling of high-speed interconnections. *IEEE Trans. Adv. Packag.* **1999**, *22*, 356–364. [CrossRef]

21. Duan, S.F.; Zhao, L.; Li, Z.B.; Zhan, H.M.; Li, C.R. Experimental and simulation study on statistical characteristics of VFTO and VFTC in GIS. *Power Syst. Technol.* **2015**, *39*, 3634–3640.

22. Du, W.; Li, Y.G.; Liu, J.M. A new VFTO whole process simulation method based on time domain finite element. *Proc. CSEE* **2014**, *34*, 3004–3012.

23. Wang, F.; Yang, M. Fast electromagnetic transient simulation for over-voltages of transmission line by high order Radau method and *V*-transformation. *IET Gener. Transm. Distrib.* **2016**, *10*, 3639–3645. [CrossRef]